Demonstration of a fully tunable entangling gate for continuous-variable one-way quantum computation

Shota Yokoyama,[1] Ryuji Ukai,[1] Seiji C. Armstrong,[1,2] Jun-ichi Yoshikawa,[1] Peter van Loock,[3] and Akira Furusawa[1,*]

[1]*Department of Applied Physics, School of Engineering, The University of Tokyo, 7-3-1 Hongo, Bunkyo-ku, Tokyo 113-8656, Japan*
[2]*Centre for Quantum Computation and Communication Technology, Department of Quantum Science, Research School of Physics and Engineering, The Australian National University, Canberra, ACT 0200, Australia*
[3]*Institute for Physics, University of Mainz, D-55128 Mainz, Germany*

We introduce a fully tunable entangling gate for continuous-variable one-way quantum computation. We present a proof-of-principle demonstration by propagating two independent optical inputs through a three-mode linear cluster state and applying the gate in various regimes. The genuine quantum nature of the gate is confirmed by verifying the entanglement strength in the output state. Our protocol can be readily incorporated into efficient multimode interaction operations in the context of large-scale one-way quantum computation, as our tuning process is the generalization of cluster-state shaping.

I. INTRODUCTION

The quantum computer promises an impressive speedup in certain problems such as prime factorization [1]. Measurement-based quantum computation (MBQC) is one approach to processing quantum information, attractive due to its relative ease of use once a suitable resource state has been prepared. In MBQC, unitary operations are performed via preprepared multipartite entangled resource states, referred to as cluster states [2–4]. Sufficiently large cluster states are first prepared before being appropriately reshaped for any specific operations. Arbitrary unitary operations are implemented by the precise selection of measurement bases and outcome-dependent feedforward operations.

To date there have been several demonstrations of MBQC, predominantly in quantum optics. Optical experiments performed in a continuous-variable (CV) setting benefit from deterministic state generation as well as deterministic implementations of Gaussian operations. The cluster states that facilitate MBQC can be generated via linear optics [5–8]. Four-mode and six-mode cluster states have been used to implement arbitrary single-mode Gaussian gates [9], a two-mode Gaussian gate [10], and a gate sequence of these two [11]. Reshaping a cluster state [12] is possible through quantum erasing [13] and wire shortening [14], which correspond to erasing and preserving the interaction gains between the nodes of the cluster state, respectively. Recently, large-scale [7] and ultralarge-scale [8] cluster states have been generated by multiplexing in the frequency and time domains, respectively, both based on the same theoretical proposal [15,16].

Present techniques for shaping a cluster are inherently inefficient due to the lack of control over the interaction strength. For example, the fixed-strength entangling gate demonstrated in Ref. [10] cannot have its entanglement strength tuned, and therefore it cannot completely make use of the underlying structure of the cluster state [17].

In this paper, we present a fully tunable entangling gate for CV one-way quantum computation and experimentally demonstrate a proof-of-principle implementation. Our tunable gate can be interpreted as a generalized instance of cluster-state reshaping, which we name cluster gain tuning. Our implementation involves propagating two independent quantized optical modes (qumodes) through a three-mode linear cluster state while implementing the gate at various strengths. The tunable interaction gain in the resource cluster state is teleported onto the two-mode input state [18], thus appearing at the output and becoming manifest as a certain form of entanglement.

II. PROTOCOL FOR TUNABLE ENTANGLING GATES VIA CLUSTER GAIN TUNING

Our quantum states are represented by the quadrature operators $(\hat{x}_j, \hat{p}_j)$ of an electric field (annihilation) operator $\hat{a}_j = \hat{x}_j + i\hat{p}_j$, where the subscript j denotes the jth optical mode. These quadrature operators play the roles of position and momentum operators of the corresponding harmonic oscillator, and hence they are canonically conjugate variables: $[\hat{x}_j, \hat{p}_k] = i/2\,\delta_{jk}$ ($\hbar = 1/2$), where δ_{jk} is the Kronecker delta. A CV cluster state is defined, in the ideal case, through its zero eigenvalues for certain linear combinations of the canonical operators, so-called nullifiers,

$$\hat{p}_{Cj} - \sum_{k \in N_j} \hat{x}_{Ck} \equiv \hat{\delta}_j, \tag{1}$$

where N_j refers to the nearest-neighbour nodes of node j in the sense of a general graph [19]. Arbitrary bonds in CV cluster states are generated by applying controlled-PHASE gates $\hat{C}_{Zjk} = e^{2i\hat{x}_j\hat{x}_k}$ on pairs of nodes, which are initialized as momentum eigenstates with 0 eigenvalues in the limit of infinite squeezing [4]. This can be understood mathematically as the transformation of nullifiers,

$$\left(\sum_{k \in N_j} \hat{C}_{Zjk}\right)\hat{p}_{Cj}\left(\sum_{k \in N_j} \hat{C}_{Zjk}^{\dagger}\right) = \hat{\delta}_j. \tag{2}$$

*akiraf@ap.t.u-tokyo.ac.jp

The controlled-PHASE gates will be generalized to include arbitrary, real gain values, $\hat{C}_{Zjk}(g) \equiv e^{2ig\hat{x}_j\hat{x}_k}$, leading to certain weighted (real-valued) graph states, with $g = 1$ as the special case of unweighted graph states. More generally, any physical graph state can be described by complex weights and a complex adjacency matrix (including self-loops), corresponding to a set of non-Hermitian nullifiers, where the eigenvalue (nullifier) conditions are still exactly fulfilled even for finite squeezing [20]. However, instead of complex weights in the following, we describe physical, finitely squeezed cluster states allowing nonzero excess noise in the Hermitian nullifier operators $\hat{\delta}_j$ [10].

After the preparation of a generic cluster state, the undesired bonds and nodes of the cluster can be erased by means of measurement and feedforward, applying the quantum eraser [13]. For example, the three-mode linear cluster state shown at the top in Fig. 1(a), which is the resource state for our demonstration of the tunable entangling gate, has bonds ($C1$-$C2$) and ($C2$-$C3$). By measuring the position operator of node $C2$ ($\hat{x}_{C2}$) and subtracting the measurement outcome from the momentum operators of the nearest-neighbor nodes ($C1$ and $C3$), the bonds are erased and the two modes end up in a separable state [bottom left, Fig. 1(a)]. On the other hand, a node can be deleted while keeping the bond up to local phase rotations, which is called wire shortening [14]. By measuring the momentum operator of node $C2$ ($\hat{p}_{C2}$) in the same three-mode linear cluster state and subtracting the measurement outcome from the position operator of a nearest-neighbor node (either $C1$ or $C3$), the resulting two-mode state becomes an Einstein-Podolsky-Rosen state or a two-mode cluster state up to local phase rotations [bottom right, Fig. 1(a)]. The two procedures described above can then be regarded as two extreme cases of cluster shaping. Here we generalize these procedures by considering intermediate operations between them, where we can tune the cluster gain between two cluster nodes via the measurement of the center node up to local unitaries.

We now discuss our implementation of cluster gain tuning on a three-mode linear cluster state. Here we consider a measurement of the observable $\hat{x}_{C2}\cos\theta - \hat{p}_{C2}\sin\theta$ on cluster node $C2$, where $\theta = 0°$ and $90°$ correspond to erasing and wire shortening, respectively. By subtracting the measurement outcome rescaled by $1/\cos\theta$ from the momentum operators of nearest-neighbor nodes ($C1$ and $C3$), the nullifiers of the resulting state become

$$\hat{\delta}_1' \equiv \hat{p}_{C1} - (\hat{x}_{C1} + \hat{x}_{C3})\tan\theta \quad \text{and} \qquad (3a)$$

$$\hat{\delta}_3' \equiv \hat{p}_{C3} - (\hat{x}_{C1} + \hat{x}_{C3})\tan\theta \qquad (3b)$$

[bottom center, Fig. 1(a)] (see Appendix B). In analogy with Eq. (2), they correspond to the transformation of nullifiers:

$$\hat{T}_{ZC1C3}(\theta)\hat{p}_{C1}\hat{T}^{\dagger}_{ZC1C3}(\theta) = \hat{\delta}_1', \qquad (4a)$$

$$\hat{T}_{ZC1C3}(\theta)\hat{p}_{C3}\hat{T}^{\dagger}_{ZC1C3}(\theta) = \hat{\delta}_3', \qquad (4b)$$

where the definition of the unitary operator is

$$\hat{T}_{Zjk}(\theta) \equiv e^{i(\hat{x}_j + \hat{x}_k)^2 \tan\theta}, \qquad (5)$$
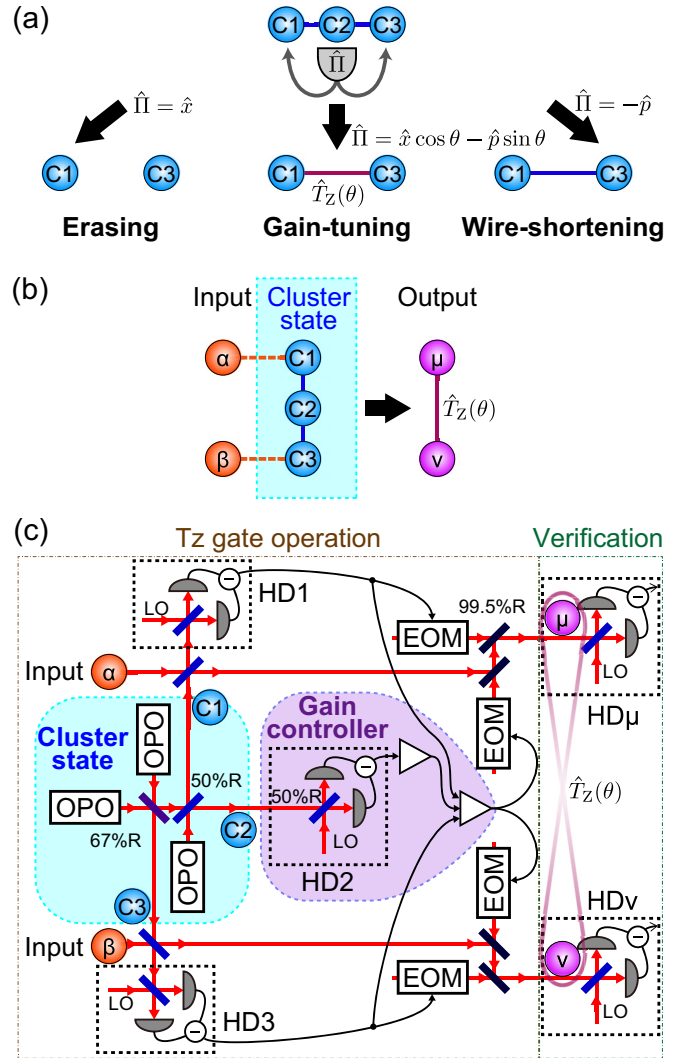

FIG. 1. (Color online) (a) Cluster-state shaping. Top: An initial three-mode linear cluster state. Bottom left: Quantum erasing. Bottom center: Interaction gain tuning. Bottom right: Wire shortening. Hemispheric objects next to the nodes (circles) and arrows represent measurements and feedforwards regarding measurement outcomes, respectively. $\hat{\Pi}$ is the measurement observable. (b) Abstract illustration of our experiment. Dashed lines represent beam-splitter coupling. (c) Schematic of our experimental setup. EOM, electro-optical modulator; HD, homodyne detector; LO, local oscillator; OPO, optical parametric oscillator; r%R, r% reflectivity beam splitter.

and therefore the resulting state corresponds to the application of the gate on two momentum eigenstates with zero eigenvalues. We name this operation the *fully tunable entangling gate* T_Z, which has the tunable interaction parameter $\tan\theta$. Since the measurement angle θ can be set arbitrarily from $-90°$ to $90°$, the T_Z gate can have an arbitrary real value of the interaction parameter $\tan\theta$. The T_Z gate consists of two quadratic phase gates for individual modes ($e^{i\hat{x}_j^2\tan\theta}, e^{i\hat{x}_k^2\tan\theta}$) [21] and a controlled-PHASE gate [$C_{Zjk}(\tan\theta) = e^{2i\hat{x}_j\hat{x}_k\tan\theta}$] with the arbitrary interaction parameter $\tan\theta$. The above cluster gain tuning allows for the generation of weighted gain cluster states from larger unweighted cluster states, while additional single-mode operations can be absorbed in the

measurements at the latter process in order to perform larger one-way quantum computations.

The tunable entangling gate is constructed by combining the cluster gain tuning scheme with two input states as shown in Fig. 1(b). Two input states in modes α and β are teleported to modes $C1$ and $C3$ by half Bell measurements and cluster gain tuning, resulting in the T_Z gate operation's being teleported onto the input states [18].

In the following we describe the above procedure taking into account the excess noises $\hat{\delta}_j$ due to finite squeezing. Each input mode (α or β) is coupled with a side mode in the cluster state via a balanced beam splitter. Then one output arm of each of the two mixing beam splitters as well as the center mode in the cluster state is measured by means of homodyne detection. The measured observables correspond to

$$\hat{s}_1 \equiv \hat{x}_{\alpha'} = \frac{1}{\sqrt{2}}(\hat{x}_\alpha - \hat{x}_{C1}), \tag{6a}$$

$$\hat{s}_3 \equiv \hat{x}_{\beta'} = \frac{1}{\sqrt{2}}(\hat{x}_\beta - \hat{x}_{C3}), \quad \text{and} \tag{6b}$$

$$\hat{s}_2(\theta) \equiv \hat{x}_{C2}\cos\theta - \hat{p}_{C2}\sin\theta, \tag{6c}$$

where θ is the measurement angle of homodyne detection on the center mode. We use primes to mark the modes after each beam-splitter interaction. The quadratures of the remaining parts are

$$\hat{x}_{C1'} = \frac{1}{\sqrt{2}}(\hat{x}_\alpha + \hat{x}_{C1}), \quad \hat{p}_{C1'} = \frac{1}{\sqrt{2}}(\hat{p}_\alpha + \hat{p}_{C1}), \tag{7a}$$

$$\hat{x}_{C3'} = \frac{1}{\sqrt{2}}(\hat{x}_\beta + \hat{x}_{C3}), \quad \hat{p}_{C3'} = \frac{1}{\sqrt{2}}(\hat{p}_\beta + \hat{p}_{C3}). \tag{7b}$$

Measurement bases (6a)–(6c) and nullifiers of an initial state determine feedforward operations to erase classical correlations derived from the measurements. Based on the measurement outcomes, we perform the following feedforward operations onto the rest of the states,

$$\hat{X}_{C1'}(\hat{s}_1)\hat{Z}_{C1'}\left((\hat{s}_1 + \hat{s}_3)\tan\theta - \frac{\hat{s}_2(\theta)}{\sqrt{2}\cos\theta}\right) \quad \text{and} \tag{8a}$$

$$\hat{X}_{C3'}(\hat{s}_3)\hat{Z}_{C3'}\left((\hat{s}_1 + \hat{s}_3)\tan\theta - \frac{\hat{s}_2(\theta)}{\sqrt{2}\cos\theta}\right), \tag{8b}$$

where $\hat{X}_k(s) = e^{-2is\hat{p}_k}$ and $\hat{Z}_k(s) = e^{2is\hat{x}_k}$ are the Weyl-Heisenberg position and momentum displacement operators for the state labeled by k, respectively. Position displacements are terms for the teleportation of input modes. On the other hand, momentum displacements according to the measurement outcome for mode $C2$ arise from cluster gain tuning. The rest corresponds to correction terms in order to accomplish teleportation and cluster gain tuning simultaneously. The effects of these displacement operators correspond to additions and subtractions for quadratures [see Appendix A],

$$\hat{x}_\mu \equiv \hat{x}_{C1'} + \hat{s}_1 = \sqrt{2}\hat{x}_\alpha, \tag{9a}$$

$$\hat{p}_\mu \equiv \hat{p}_{C1'} + (\hat{s}_1 + \hat{s}_3)\tan\theta - \frac{\hat{s}_2(\theta)}{\sqrt{2}\cos\theta}$$

$$= \frac{1}{\sqrt{2}}[\hat{p}_\alpha + (\hat{x}_\alpha + \hat{x}_\beta)\tan\theta + \hat{\delta}_1 + \hat{\delta}_2\tan\theta], \tag{9b}$$

$$\hat{x}_\nu \equiv \hat{x}_{C3'} + \hat{s}_3 = \sqrt{2}\hat{x}_\beta, \tag{9c}$$

$$\hat{p}_\nu \equiv \hat{p}_{C3'} + (\hat{s}_1 + \hat{s}_3)\tan\theta - \frac{\hat{s}_2(\theta)}{\sqrt{2}\cos\theta}$$

$$= \frac{1}{\sqrt{2}}[\hat{p}_\beta + (\hat{x}_\alpha + \hat{x}_\beta)\tan\theta + \hat{\delta}_3 + \hat{\delta}_2\tan\theta], \tag{9d}$$

where we refer to the two output modes as μ and ν in order to distinguish them from the input modes denoted α and β. Consequently, the input-output relation in the Heisenberg picture is given by

$$\hat{\boldsymbol{\xi}}_{\mu\nu} = \begin{pmatrix} \boldsymbol{S} & \boldsymbol{0} \\ \boldsymbol{0} & \boldsymbol{S} \end{pmatrix} \begin{pmatrix} \boldsymbol{I} + \boldsymbol{T}(\theta) & \boldsymbol{T}(\theta) \\ \boldsymbol{T}(\theta) & \boldsymbol{I} + \boldsymbol{T}(\theta) \end{pmatrix} \hat{\boldsymbol{\xi}}_{\alpha\beta} + \hat{\boldsymbol{\delta}} \tag{10}$$

$$= (\hat{S}_\alpha\hat{S}_\beta\hat{T}_{Z\alpha\beta}(\theta))^\dagger \hat{\boldsymbol{\xi}}_{\alpha\beta}(\hat{S}_\alpha\hat{S}_\beta\hat{T}_{Z\alpha\beta}(\theta)) + \hat{\boldsymbol{\delta}}, \tag{11}$$

where

$$\hat{\boldsymbol{\xi}}_{\mu\nu} = \begin{pmatrix} \hat{x}_\mu \\ \hat{p}_\mu \\ \hat{x}_\nu \\ \hat{p}_\nu \end{pmatrix}, \quad \hat{\boldsymbol{\xi}}_{\alpha\beta} = \begin{pmatrix} \hat{x}_\alpha \\ \hat{p}_\alpha \\ \hat{x}_\beta \\ \hat{p}_\beta \end{pmatrix}, \tag{12}$$

$$\boldsymbol{S} = \begin{pmatrix} \sqrt{2} & 0 \\ 0 & 1/\sqrt{2} \end{pmatrix}, \quad \boldsymbol{T}(\theta) = \begin{pmatrix} 0 & 0 \\ \tan\theta & 0 \end{pmatrix}, \tag{13}$$

$\boldsymbol{I}$ is the 2×2 identity matrix, and

$$\hat{\boldsymbol{\delta}} = \begin{pmatrix} 0 \\ \hat{\delta}_1 + \hat{\delta}_2\tan\theta \\ 0 \\ \hat{\delta}_3 + \hat{\delta}_2\tan\theta \end{pmatrix} \tag{14}$$

are excess noise terms for imperfect resource squeezing. There are local squeezing operations $\hat{S}_j = e^{-i\ln 2(\hat{x}_j\hat{p}_j + \hat{p}_j\hat{x}_j)/2}$ in addition to the teleported T_Z gate. These -3.0-dB p-squeezing operations are due to the input coupling with a balanced beam splitter. A half-teleportation with a beam-splitter coupling corresponds to a squeezing gate [22,23]. Note that it can be eliminated by adding an additional coupling node at the edge of cluster states, by which full quantum teleportation with full Bell measurements is performed into the cluster state instead of half-teleporation with half Bell measurements [17].

In order to verify the entangling capability of the T_Z gate, we now consider the case where both input states are coherent states. Since there are various measurable quantum correlations depending on the measurement basis $\hat{s}_2(\theta)$, we evaluate the entanglement with the minimum symplectic eigenvalue $\tilde{\lambda}_-$ of the partially transposed covariance matrix of the output state [24], which is invariant under arbitrary local unitary operators. This corresponds to the logarithmic negativity, which gives $E_N = \max[0, -\ln(4\tilde{\lambda}_-)]$ for the case of Gaussian states and which is an entanglement measure invariant under local unitary operations [25]. The covariance matrix is given by $V \equiv \frac{1}{2}\langle\{\hat{\boldsymbol{\xi}}, \hat{\boldsymbol{\xi}}\}\rangle$, where $\{\hat{\boldsymbol{u}}, \hat{\boldsymbol{v}}\} \equiv \hat{\boldsymbol{u}}\hat{\boldsymbol{v}}^T + (\hat{\boldsymbol{v}}\hat{\boldsymbol{u}}^T)^T$ [20].

For our setup the minimum symplectic eigenvalue becomes

$$\tilde{\lambda}_- = \frac{1}{4}\{1 + 2t^2 + (2 + 3t^2)e^{-2r}$$

$$- \sqrt{4t^2[1 + t^2 + (2 + 3t^2)e^{-2r}] + [(1 + 3t^2)e^{-2r}]^2}\}^{1/2}, \tag{15}$$

where $t = \tan\theta$. It can be calculated by means of the excess noise terms with $\hat{\delta}_1 = \sqrt{2}e^{-r}\hat{p}_1^{(0)}$, $\hat{\delta}_2 = \sqrt{3}e^{-r}\hat{p}_2^{(0)}$, and $\hat{\delta}_3 = \frac{1}{\sqrt{2}}e^{-r}\hat{p}_1^{(0)} + \sqrt{\frac{3}{2}}e^{-r}\hat{p}_3^{(0)}$, where $e^{-r}\hat{p}_j^{(0)}$ is a squeezed quadrature of the jth resource squeezed-vacuum mode before the beam-splitter network. Here we assume that all three modes have the same level of squeezing r, for simplicity. The asymmetric case is easily derived in a similar manner. The ideal (unphysical) cluster state is obtained in the limit $r \to \infty$.

The positivity under partial transposition (PPT criterion) is a necessary (and sufficient, in the case of two-mode Gaussian states) measure for the separability of a state [26]. Thus, the output states of our setup are entangled if $\tilde{\lambda}_-$ is below 1/4. Furthermore, the closer $\tilde{\lambda}_-$ is to 0, the stronger is the entanglement in the output states. With respect to our T_Z gate, $\tilde{\lambda}_-$ becomes smaller as we increase the interaction parameter $\tan\theta$.

III. EXPERIMENT

A schematic of our experimental setup is shown in Fig. 1(c). The light source is a continuous-wave Ti:sapphire laser with a wavelength of 860 nm and a power of about 1.7 W. The quantum states to be processed are qumodes at 1-MHz sidebands of the laser beam. The resource cluster state is prepared by combining three squeezed vacuum states on two beam splitters, each generated by a subthreshold optical parametric oscillator (OPO). We mainly employ the experimental techniques described in Ref. [27] for the feedforward of measurement results through classical channels. Note that the tunable interaction parameter $t = \tan\theta$ of the T_Z gate is accessed via the relative phase θ between the signal beam and the reference local oscillator beam at the homodyne-2 detection station (HD-2). The relative phase is precisely controlled via the voltage sent to a piezoelectric transducer (PZT) attached to a mirror. Squeezing levels of the resource squeezed vacuum states are about -4.5 dB. The propagation losses from the optical parametric oscillators to the homodyne detectors are 3% to 9%. The detectors' quantum efficiencies are 99%, and the interference visibilities are 96% on average.

In order to evaluate our gate we measure the powers of the quadratures at the homodyne detectors with a spectrum analyzer. The measured frequency is 1 MHz, with a resolution bandwidth of 30 kHz and video bandwidth of 300 Hz. For each quadrature, 101 data points are taken, with a sweep time of 0.05 s, while this is repeated 10 times for averaging. Standard errors in these averaged measurements are less than 0.06 dB. In the case of coherent state inputs, we average over even more measurements, leading to standard errors of <0.01 dB. Note that no corrections are applied for any experimental losses.

In Figs. 2(a)–2(d), we visualize the phase-space distributions of the output Gaussian states by ellipses for seven interaction parameters, $t = \tan\theta \in \{0, \frac{1}{5}, \frac{1}{2}, \frac{1}{\sqrt{2}}, 1, \sqrt{2}, 2\}$, for vacuum state inputs. These interaction parameters correspond to the measurement angles $\theta \in \{0.0°, 11.3°, 26.6°, 35.3°, 45.0°, 54.7°, 63.4°\}$. The second moments are expressed by the size of the phase-space ellipse, which corresponds to the cross section of the quantum

(a) Ideal case. HDμ

(b) Ideal case. HDv

(c) Experiment. HDμ

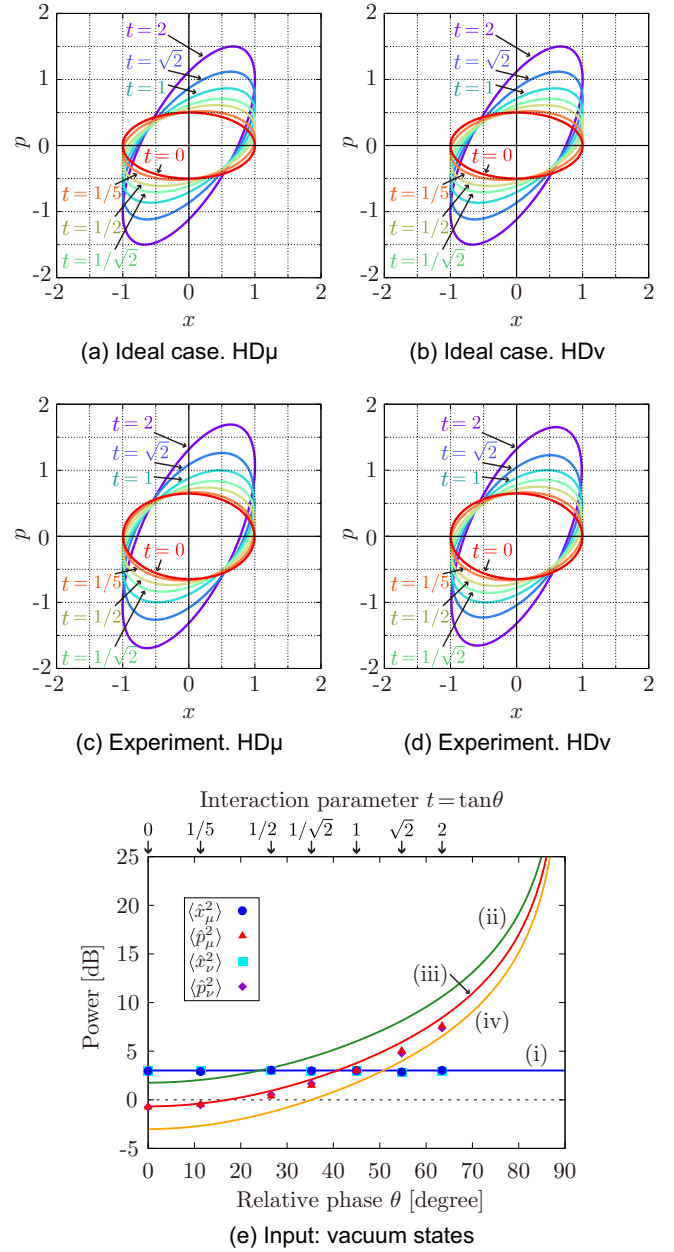(d) Experiment. HDv

(e) Input: vacuum states

FIG. 2. (Color online) Output states for a T_Z gate operating at several interaction parameters, $t = \tan\theta \in \{0, 1/5, 1/2, 1/\sqrt{2}, 1, \sqrt{2}, 2\}$, employing two vacuum inputs. (a–d) Phase-space distributions. The second moments of Gaussian Wigner functions are represented by ellipses. Long and short radii correspond to $\sqrt{2}$ times standard deviations in the corresponding directions. (a, b) Theoretical predictions for the ideal case with infinite resource squeezing. (c, d) Experimental results computed from the measured variances of $\hat{x}_j$, $\hat{p}_j$, and $(\hat{x}_j \pm \hat{p}_j)/\sqrt{2}$, where $j \in \{\mu, \nu\}$. (e) Measured variances of $\hat{x}_j$, $\hat{p}_j$. The horizontal axis is the relative phase θ between the signal beam and the local oscillator beam at HD-2, which determines the interaction parameter, as $t = \tan\theta$. Colored lines show the theoretical predictions of (i) $\langle\hat{x}_j^2\rangle$, (ii) $\langle\hat{p}_j^2\rangle$ without squeezing, (iii) $\langle\hat{p}_j^2\rangle$ with -4.5-dB resource squeezing, and (iv) $\langle\hat{p}_j^2\rangle$ with infinite squeezing (unphysical, ideal case). Error bars are omitted, because they are very small compared to the scale of the vertical axis.

state's Wigner function. Long and short radii correspond to $\sqrt{2}$ times standard deviations in the corresponding directions.

The theoretical predictions of the ideal case with infinite resource squeezing ($r \to \infty$) are shown in Figs. 2(a) and 2(b). Here, we see that the $\hat{x}$ quadrature amplitudes remain fixed, while the $\hat{p}$ quadrature amplitudes increase with larger interaction parameter values. The broadening in $\hat{p}$ is due to the uncorrelated quantum fluctuations of both $\hat{x}_{\alpha}$ and $\hat{x}_{\beta}$ being added to $\hat{p}_{\alpha}$ and $\hat{p}_{\beta}$ by the interaction-parameter-dependent T_{Z} gate. Note that the additional local squeezing operations decrease these fluctuations. The variances of $\hat{x}_{\alpha}$ and $\hat{x}_{\beta}$ are fixed at twice the shot noise level (SNL) from the additional local squeezing and are not dependent on the interaction parameter.

The experimental results are shown in Figs. 2(c) and 2(d), which are calculated from the measured variances of $\hat{x}_j$, $\hat{p}_j$, and $(\hat{x}_j \pm \hat{p}_j)/\sqrt{2}$, where $j \in \{\mu, \nu\}$. We assume a Gaussian distribution and 0 mean value. Each of the two output modes has a nearly identical phase-space distribution with respect to the other, indicative of the high level of symmetry in our optical mode matching. We see a slight broadening in $\hat{p}$ compared to the ideal case predicted by theory, due to the finite resource squeezing which couples in excess noise, while $\hat{x}$ remains unaffected, in accordance with $\hat{\boldsymbol{\delta}}$ in Eq. (14).

In order to compare them with the following results, the measured variances of $\hat{x}_{\alpha}$, $\hat{x}_{\beta}$, $\hat{p}_{\alpha}$, and $\hat{p}_{\beta}$ are plotted in Fig. 2(e). The horizontal axis is the relative phase θ between the signal beam and the local oscillator beam at HD-2. The variances of $\hat{x}$ are 3.0 dB above the SNL independent of the resource squeezing level r and the interaction parameter $\tan \theta$ as expected from the theory expressed by the blue line, (i), while $\hat{p}$ depends on them. The green line, (ii), represents the theoretical predictions for zero resource squeezing, while the orange line, (iv), represents infinite squeezing. Finite squeezing values appear between these two extremes, and we find that our experimental results are close to the theoretical prediction of -4.5-dB resource squeezing, as indicated by the red line, (iii). These results indicate a good qualitative agreement with the theoretical predictions.

Next, we replace one of the input vacuum states by coherent states, allowing us to verify the input-output relationship based on the assumption that the gate has a linear response. The powers of the input amplitude quadratures are individually measured in advance, corresponding to 13.8 dB for mode α and 16.9 dB for mode β, respectively, compared to the SNL.

In analogy with Fig. 2, Fig. 3(a) shows the powers of the output quadratures for an input coherent state α and an input vacuum state β. The output quadrature powers are shown as a function of the relative phase θ between the signal beam and the local oscillator beam at HD-2, which determines the interaction parameter $\tan \theta$. Theoretical predictions are shown as lines and experimental data as markers. The predictions are calculated from the measured input coherent amplitude with a resource squeezing level of -4.5 dB. We observe fixed power increases in $\hat{x}$- and θ-dependent increases in $\hat{p}$. The power of $\hat{x}_{\mu}$ increases by 3.0 dB above the inital 13.8 dB (corresponding to about 17 dB above the SNL; blue symbols), which is due to the additional local squeezing operation. The power of $\hat{x}_{\nu}$ is the same as the case of two vacuum inputs (corresponding to 3.0 dB above the SNL; cyan symbols). $\hat{p}_{\mu}$ and $\hat{p}_{\nu}$ experience
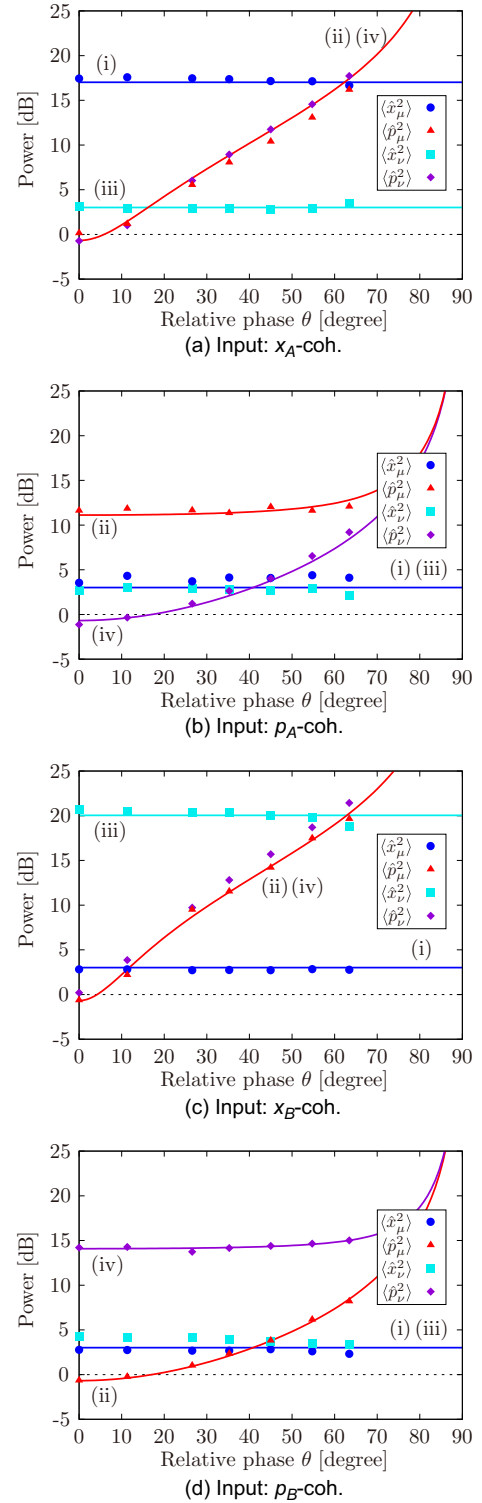

FIG. 3. (Color online) Powers at the outputs from two coherent inputs with several interaction parameters. Horizontal axes are the relative phases θ between the signal beam and the local oscillator beam at HD-2, which are related to the interaction parameters $\tan \theta$. (a–d) ($\langle \hat{x}_{\alpha} \rangle$, $\langle \hat{p}_{\alpha} \rangle$, $\langle \hat{x}_{\beta} \rangle$, and $\langle \hat{p}_{\beta} \rangle$) are $(a,0,0,0)$, $(0,a,0,0)$, $(0,0,b,0)$, and $(0,0,0,b)$, where a^2 and b^2 correspond to 13.8 and 16.9 dB above the shot noise level, respectively. (i), (ii), (iii), and (iv) Theoretical predictions of (i) $\langle \hat{x}_{\mu}^2 \rangle$, (ii) $\langle \hat{p}_{\mu}^2 \rangle$, (iii) $\langle \hat{x}_{\nu}^2 \rangle$, and (iv) $\langle \hat{p}_{\nu}^2 \rangle$ with -4.5-dB resource squeezing. coh., coherent state. Error bars are omitted, because they are very small compared to the scale of the vertical axis.
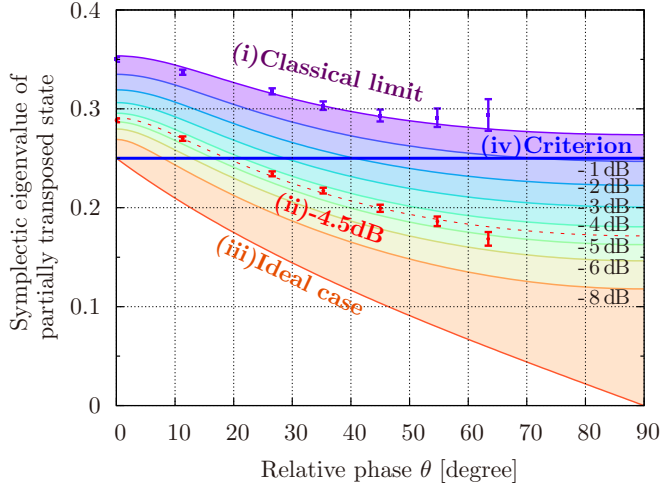
FIG. 4. (Color online) Dependence of the entanglement at the outputs on the interaction parameters of the T_Z gate. The horizontal axis corresponds to the relative phase θ between the signal beam and the local oscillator beam at HD-2, which determines the interaction parameter $\tan\theta$. The vertical axis corresponds to the symplectic eigenvalues of the partially transposed covariance matrix of the output state, connected to a measure of entanglement (see text). (i) Without squeezing, (ii) with -4.5-dB resource squeezing, (iii) with infinite squeezing (unphysical, ideal case), and (iv) quantum boundary; values below satisfy a sufficient condition for entanglement. Error bars show standard errors.

larger increases in power relative to the case of vacuum inputs in Fig. 2(e), due to the increasing contribution of the nonzero coherent amplitude of $\hat{x}_\alpha$ via the T_Z gate. Similarly, Figs. 3(b), 3(c), and 3(d) show the results for a nonzero coherent amplitude in the $\hat{p}_\alpha$, $\hat{x}_\beta$, and $\hat{p}_\beta$ input quadratures, respectively. The T_Z gate behaves as predicted, with the sum of $\hat{x}_\alpha$ and $\hat{x}_\beta$ appropriately appearing in both $\hat{p}_\mu$ and $\hat{p}_\nu$ quadratures, as a function of the interaction parameters. The small discrepancies between our experimental results and the theoretical predictions are caused by the (slightly unbalanced) propagation losses and nonunity homodyne detections.

Finally, the entanglement strength is quantified in Fig. 4. Shown there is the set of symplectic eigenvalues $\tilde{\lambda}_-$ of the partially transposed covariance matrices corresponding to the output states. These are calculated from the variances of the output quadratures for vacuum inputs (see Ref. [28] for details) and are displayed as a function of the T_Z interaction parameter (as determined by the relative phase of homodyne detection). Note that the results of covariance matrices satisfy the physicality condition $V + (i/4)\,\Omega \geqslant 0$, where Ω is a direct sum of $\begin{pmatrix} 0 & -1 \\ 1 & 0 \end{pmatrix}$ [29,30]. The theoretical predictions for the experiment with and without resource squeezing are represented by the theoretical curves, (ii) and (i), respectively. We observe the remarkable feature of an enhancement in entanglement strength dependent on the interaction parameter. The entangling criterion is satisfied for parameter values of $\tan\theta = \frac{1}{2}$, $\frac{1}{\sqrt{2}}$, 1, $\sqrt{2}$, and 2 when the resource state is squeezed. Conversely, without squeezing, the symplectic eigenvalues never cross the quantum boundary for any value of interaction parameter.

IV. CONCLUSION

In conclusion, we have proposed and experimentally demonstrated a fully tunable T_Z gate for CV one-way quantum computation. Our proof-of-principle demonstration employs a three-mode linear cluster state as a resource for implementing a new cluster gain tuning protocol. The ability of the gate to produce entanglement at the output is verified via the symplectic eigenvalues of the partially transposed covariance matrix of the output for the case of two coherent input states. The interaction parameter at the gate and, accordingly, the entanglement strength in the output state are accurately tuned by a corresponding tuning of the set of measurement bases. Since our gate can be directly incorporated into large-scale one-way quantum computation schemes, it may facilitate efficient implementations of MBQC with cluster states.

APPENDIX A: MATHEMATICAL TREATMENT OF FEEDFORWARD

We consider a situation where some observable $\hat{s}_c$ of a control mode c is measured and then the outcome s is used for feedforward to a target mode t as a displacement operation $\hat{Z}_t(s) = e^{2is\hat{x}_t}$. As its name suggests, a displacement operator $\hat{Z}_t(s)$ displaces a quadrature operator in the $\hat{p}$ direction,

$$\hat{Z}_t^\dagger(s)\hat{x}_t\hat{Z}_t(s) = \hat{x}_t, \quad \hat{Z}_t^\dagger(s)\hat{p}_t\hat{Z}_t(s) = \hat{p}_t + s. \quad \text{(A1)}$$

It is a well-known fact, as depicted in Fig. 5, that a measurement in the middle of successive unitary gates can be moved to the last by appropriately replacing the feedforward circuits with controlled gates. Based on this equivalence, here as a matter of notation, we write a $\hat{Z}_t(s)$ gate dependent on a measurement outcome s of an observable $\hat{s}_c$ as $\hat{Z}_t(\hat{s}_c) = e^{2i\hat{s}_c\hat{x}_t}$, which transforms the quadrature operators,

$$\hat{Z}_t^\dagger(\hat{s}_c)\hat{x}_t\hat{Z}_t(\hat{s}_c) = \hat{x}_t, \quad \hat{Z}_t^\dagger(\hat{s}_c)\hat{p}_t\hat{Z}_t(\hat{s}_c) = \hat{p}_t + \hat{s}_c. \quad \text{(A2)}$$

As a special case, when $\hat{s}_c = \hat{x}_c$, the equivalent gate $\hat{Z}_t(\hat{x}_c) = e^{2i\hat{x}_c\hat{x}_t} = \hat{C}_{Zct}$ is a controlled-PHASE gate.
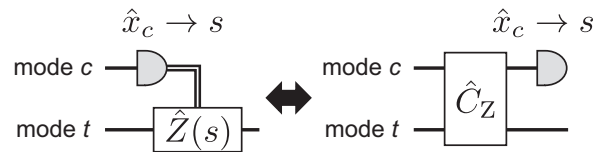

FIG. 5. Equivalent quantum circuits. Left: Executing displacement after measurement. Right: Measurement after an interaction gate.

Similarly, we can also consider the case of $\hat{x}$-direction displacement feedforward $\hat{X}_t(s) = e^{-2is\hat{p}_t}$, where the equivalent controlled gate is $\hat{X}_t(\hat{s}_c) = e^{-2i\hat{s}_c\hat{p}_t}$.

APPENDIX B: NULLIFIERS AFTER CLUSTER GAIN TUNING

In the cluster gain tuning starting from a three-mode linear cluster state in Fig. 1(a), first a center mode is measured with respect to an observable,

$$\hat{s}_2(\theta) = \hat{x}_{C2} \cos\theta - \hat{p}_{C2} \sin\theta. \quad (B1)$$

Then the outcome s_2 is used for a feedforward displacement operation $\hat{Z}_{C1}(-s_2/\cos\theta)\hat{Z}_{C3}(-s_2/\cos\theta)$, which transforms the quadratures of the remaining two modes as

$$\hat{x}'_{C1} = \hat{Z}^\dagger_{C1}\left(-\frac{\hat{s}_2(\theta)}{\cos\theta}\right)\hat{x}_{C1}\hat{Z}_{C1}\left(-\frac{\hat{s}_2(\theta)}{\cos\theta}\right) = \hat{x}_{C1}, \quad (B2a)$$

$$\hat{p}'_{C1} = \hat{Z}^\dagger_{C1}\left(-\frac{\hat{s}_2(\theta)}{\cos\theta}\right)\hat{p}_{C1}\hat{Z}_{C1}\left(-\frac{\hat{s}_2(\theta)}{\cos\theta}\right)$$

$$= \hat{p}_{C1} - \frac{\hat{s}_2(\theta)}{\cos\theta} = \hat{p}_{C1} - \hat{x}_{C2} + \hat{p}_{C2}\tan\theta, \quad (B2b)$$

$$\hat{x}'_{C3} = \hat{Z}^\dagger_{C3}\left(-\frac{\hat{s}_2(\theta)}{\cos\theta}\right)\hat{x}_{C3}\hat{Z}_{C3}\left(-\frac{\hat{s}_2(\theta)}{\cos\theta}\right) = \hat{x}_{C3}, \quad (B2c)$$

$$\hat{p}'_{C3} = \hat{Z}^\dagger_{C3}\left(-\frac{\hat{s}_2(\theta)}{\cos\theta}\right)\hat{p}_{C3}\hat{Z}_{C3}\left(-\frac{\hat{s}_2(\theta)}{\cos\theta}\right)$$

$$= \hat{p}_{C3} - \frac{\hat{s}_2(\theta)}{\cos\theta} = \hat{p}_{C3} - \hat{x}_{C2} + \hat{p}_{C2}\tan\theta. \quad (B2d)$$

Here, we define the prime quadratures as new quadratures after displacement.

In Sec. II, the nullifiers of initial three-mode cluster states are explained as follows:

$$\hat{\delta}_1 = \hat{p}_{C1} - \hat{x}_{C2}, \quad (B3a)$$

$$\hat{\delta}_2 = \hat{p}_{C2} - \hat{x}_{C1} - \hat{x}_{C3}, \quad (B3b)$$

$$\hat{\delta}_3 = \hat{p}_{C3} - \hat{x}_{C2}. \quad (B3c)$$

In fact, nullifier operators span a vector space, and an arbitrarily linear combination of the above three operators is included in the nullifier set. The dimension of the simplest nullifier vector space corresponds to the number of modes (nodes) of the cluster states. In our cluster gain tuning, the center mode in the three-mode cluster states vanishes by measurement, which reduces the degrees of freedom of the nullifier space from three to two. The remaining two-dimensional nullifier space is spanned by the following two operators:

$$\hat{\delta}'_1 = \hat{p}'_{C1} - (\hat{x}'_{C1} + \hat{x}'_{C3})\tan\theta$$

$$= (\hat{p}_{C1} - \hat{x}_{C2}) + (\hat{p}_{C2} - \hat{x}_{C1} - \hat{x}_{C3})\tan\theta$$

$$= \hat{\delta}_1 + \hat{\delta}_2\tan\theta, \quad (B4a)$$

$$\hat{\delta}'_3 = \hat{p}'_{C3} - (\hat{x}'_{C1} + \hat{x}'_{C3})\tan\theta$$

$$= (\hat{p}_{C3} - \hat{x}_{C2}) + (\hat{p}_{C2} - \hat{x}_{C1} - \hat{x}_{C3})\tan\theta$$

$$= \hat{\delta}_3 + \hat{\delta}_2\tan\theta. \quad (B4b)$$

[1] M. A. Nielsen and I. L. Chuang, *Quantum Computation and Quantum Information* (Cambridge University Press, Cambridge, UK, 2000).

[2] H. J. Briegel and R. Raussendorf, Phys. Rev. Lett. **86**, 910 (2001).

[3] R. Raussendorf and H. J. Briegel, Phys. Rev. Lett. **86**, 5188 (2001).

[4] N. C. Menicucci, P. van Loock, M. Gu, C. Weedbrook, T. C. Ralph, and M. A. Nielsen, Phys. Rev. Lett. **97**, 110501 (2006).

[5] X. Su, A. Tan, X. Jia, J. Zhang, C. Xie, and K. Peng, Phys. Rev. Lett. **98**, 070502 (2007).

[6] M. Yukawa, R. Ukai, P. van Loock, and A. Furusawa, Phys. Rev. A **78**, 012301 (2008).

[7] M. Chen, N. C. Menicucci, and O. Pfister, Phys. Rev. Lett. **112**, 120505 (2014).

[8] S. Yokoyama, R. Ukai, S. C. Armstrong, C. Sornphiphatphong, T. Kaji, S. Suzuki, J. Yoshikawa, H. Yonezawa, N. C. Menicucci, and A. Furusawa, Nature Photon. **7**, 982 (2013).

[9] R. Ukai, N. Iwata, Y. Shimokawa, S. C. Armstrong, A. Politi, J. Yoshikawa, P. van Loock, and A. Furusawa, Phys. Rev. Lett. **106**, 240504 (2011).

[10] R. Ukai, S. Yokoyama, J. Yoshikawa, P. van Loock, and A. Furusawa, Phys. Rev. Lett. **107**, 250501 (2011).

[11] X. Su, S. Hao, X. Deng, L. Ma, M. Wang, X. Jia, C. Xie, and K. Peng, Nature Commun. **4**, 2828 (2013).

[12] Y. Miwa, R. Ukai, J. Yoshikawa, R. Filip, P. van Loock, and A. Furusawa, Phys. Rev. A **82**, 032305 (2010).

[13] R. Filip, Phys. Rev. A **67**, 042111 (2003).

[14] M. Gu, C. Weedbrook, N. C. Menicucci, T. C. Ralph, and P. van Loock, Phys. Rev. A **79**, 062318 (2009).

[15] N. C. Menicucci, S. T. Flammia, and O. Pfister, Phys. Rev. Lett. **101**, 130501 (2008).

[16] N. C. Menicucci, Phys. Rev. A **83**, 062314 (2011).

[17] R. Ukai, J. Yoshikawa, N. Iwata, P. van Loock, and A. Furusawa, Phys. Rev. A **81**, 032315 (2010).

[18] S. D. Bartlett and W. J. Munro, Phys. Rev. Lett. **90**, 117901 (2003).

[19] P. van Loock, C. Weedbrook, and M. Gu, Phys. Rev. A **76**, 032321 (2007).

[20] N. C. Menicucci, S. T. Flammia, and P. van Loock, Phys. Rev. A **83**, 042335 (2011).

[21] Y. Miwa, J. Yoshikawa, P. van Loock, and A. Furusawa, Phys. Rev. A **80**, 050303(R) (2009).

[22] R. Filip, P. Marek, and U. L. Andersen, Phys. Rev. A **71**, 042308 (2005).

[23] J. Yoshikawa, T. Hayashi, T. Akiyama, N. Takei, A. Huck, U. L. Andersen, and A. Furusawa, Phys. Rev. A **76**, 060301(R) (2007).

[24] G. Adesso, A. Serafini, and F. Illuminati, Phys. Rev. A **70**, 022318 (2004).

[25] G. Vidal and R. F. Werner, Phys. Rev. A **65**, 032314 (2002).

[26] R. Simon, Phys. Rev. Lett. **84**, 2726 (2000).

[27] M. Yukawa, H. Benichi, and A. Furusawa, Phys. Rev. A **77**, 022314 (2008).

[28] S. Yokoyama, R. Ukai, J. Yoshikawa, P. Marek, R. Filip, and A. Furusawa, Phys. Rev. A **90**, 012311 (2014).

[29] S. Pirandola, A. Serafini, and S. Lloyd, Phys. Rev. A **79**, 052327 (2009).

[30] R. Simon, N. Mukunda, and B. Dutta, Phys. Rev. A **49**, 1567 (1994).